Comparative Analysis of Pilot-based Channel Estimators for DMT Systems Over Indoor Power-line Channels

José Antonio Cortés, Andrea M. Tonello[1] and Luis Díez
jaca@ic.uma.es, tonello@uniud.it, diez@ic.uma.es
Departamento de Ingeniería de Comunicaciones
University of Málaga (Spain)
[1]Dipartimento di Ingegneria Elettrica, Gestionale e Meccanica
University of Udine (Italy)

***Abstract*—This work addresses the problem of pilot-based channel estimation in DMT systems for broadband indoor power-line communications. The study is carried out over a set of measured channels. Three estimation schemes are compared: the least-squares (LS), the linear minimum mean-squared error (LMMSE) estimator and the least-mean-square (LMS) with cubic interpolation between pilot carriers. The use of a generic LMMSE design based on channel statistics derived from measurements is proposed. Performance as a function of the pilot spacing is analyzed in terms of the mean-squared error (MSE), the error probability and the attained bit-rate.**

***Keywords*—DMT, time-varying channel, channel estimation, LMMSE, LMS, power-line communications.**

I. Introduction

INDOOR power-line channels in the frequency band up to 30MHz are frequency and time-selective. Their response can be modeled as a linear periodically time-variant (LPTV) system plus an additive cyclostationary noise term [1].

Estimation of a frequency and time-selective channel in a OFDM/DMT-based system is a two-dimensional problem [2]. It has been shown that, for a fixed complexity, separate estimation in the frequency and time dimensions offers better results than 2-D estimators [3]. Channel estimation employing only frequency correlation is usually accomplished by means of the LMMSE estimator [3,4]. Its high complexity is commonly reduced by employing a low-rank approximation of the estimator matrix and by neglecting correlation between distant pilots [3]. To avoid accurate knowledge of the channel frequency correlation, the algorithm is derived under the assumption of a uniform power-delay profile channel [3].

The LMMSE has been successfully applied in the mobile radio environment. However, in indoor power-line channels its performance may be compromised because channel statistics are not precisely known. Moreover, these channels generally exhibit much higher signal to noise ratios (SNR) than the mobile radio ones, and the mismatch due to the uniform power-delay profile assumption may severely limit the system performance.

The LMS estimator is commonly used to track time-variant channels when their statistics are not accurately known. A comb-type pilot arrangement with polynomial interpolation is frequently employed [4,5]. One of the key parameters in this scheme is the step-size, which in a time-variant channel results from the trade-off between noise reduction and tracking ability.

In this paper, pilot-based channel estimation strategies based on the LMMSE criterion and on the LMS algorithm with cubic interpolation are compared. Channel statistics derived from measurements are employed in the LMMSE case with satisfactory results. Degradation caused by complexity reduction techniques of the LMMSE estimator is evaluated. Performance of the LMS-based estimator is analyzed as a function of the step-size. The study is carried out over a set of measured channels whose statistical characterization can be found in [1].

The paper is organized as follows. Section II describes the channel model and details the estimation algorithms employed with both cases. Performance analysis is presented in section III and main conclusions are drawn in section IV.

II. System Description

A. System Model

The simplified block diagram of an N carriers DMT receiver with pilot-based channel estimation using a comb-type arrangement is shown in Fig. 1. After removing the cyclic prefix, the $2N$ real-valued samples of the received symbols are fed into the DFT. Due to the hermitian symmetry of the DMT signal, it holds that only DFT outputs with indexes $0 \le k \le N$ are passed to the next stage and that carriers $k = 0$ and $k = N$ do only transmit real values [6]. A total of N_P pilots are inserted in each transmitted symbol, one out of p carriers. The first carrier is always selected as a pilot and, when polynomial interpolation is employed, the last carrier is also

This work has been supported in part by the Spanish Ministry of Educación y Ciencia under CYCIT Project Nº TIC2003-06842.

used as an additional pilot to minimize edge effects. The phase compensation blocks are employed in the LMMSE case to compensate for the time domain delay between the actual channel and the one for which channel statistics where computed [4]. Similarly, when the LMS is used, a time domain delay in the impulse response (due to the symbol synchronization algorithm) produces a phase rotation in the frequency response that severely degrades the performance of the interpolation process. Hence, once the channel amplitudes at the pilot carriers have been estimated, the phase rotation is removed before interpolation is accomplished and reintroduced in the obtained channel amplitudes.

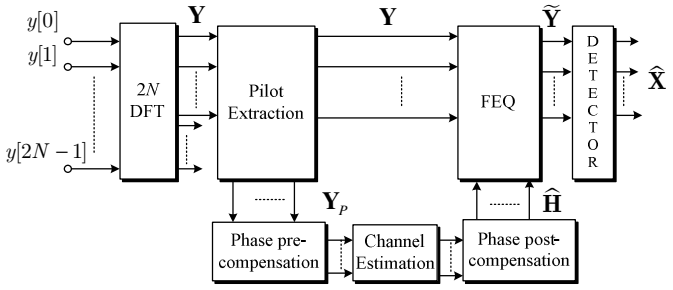

Fig. 1. Simplified block diagram of the receiver.

B. Channel Model

Simulations presented in this work have been carried out over a set of 24 channels measured in the frequency band from 1MHz to 20MHz in two indoor scenarios: 12 in an apartment of about 80m^2 and 12 in a detached house of about 300m^2. Statistical parameters of the employed channel responses and noise instantaneous power spectral densities (PSD) can be found in [1].

Transmitted carriers occupy the band from 2.5MHz to 18.5MHz and the sampling frequency is fixed to 50MHz. Two representative channels have been selected to show results. Table I shows their corresponding mean (time and frequency) SNR for a transmitted PSD of -20dBm/kHz; the mean Doppler spread, computed as described in [1], and the mean coherence bandwidth at 0.9. To allow the comparison of the MSE obtained in channels with different mean attenuation, channel frequency responses are normalized by their energy. Since, noise PSD's are correspondingly scaled, this implies no loss of generality.

TABLE I
MEAN COHERENCE BANDWIDTH, DOPPLER SPREAD AND SNR VALUES OF THE SELECTED CHANNELS

Channel	Coherence Bandwidth (kHz)	Doppler Spread (Hz)	SNR (dB)
Ch. 1	97.66	159.60	38.91
Ch. 2	170.90	67.90	24.39

C. LMMSE Estimator

Let's consider a DMT system with a sufficiently long cyclic prefix and a number of carriers small enough to assume that the channel is essentially constant during each symbol. When the noise is stationary, the LMMSE estimator of the channel frequency response yields the N components column vector [3,4]

$$\widehat{\mathbf{H}}_{LMMSE} = \mathbf{R}_{HP}\left(\mathbf{R}_{PP} + \boldsymbol{\sigma}_U^2\left(\mathbf{X}_P\mathbf{X}_P^H\right)^{-1}\right)^{-1}\widehat{\mathbf{H}}_{LS}, \quad (1)$$

where $(\cdot)^H$ denotes the Hermitian transpose, $\boldsymbol{\sigma}_U^2 = diag\left\{\sigma_{U_{p-1}}^2, \sigma_{U_{2p-1}}^2, \cdots, \sigma_{U_{N_p\cdot p-1}}^2\right\}$, where $\sigma_{U_{mp-1}}^2$ is the noise variance in carrier $mp-1$, $\mathbf{X}_P$ is a diagonal matrix with the complex data transmitted in the pilot carriers, $\mathbf{Y}_P$ is the N_P components column vector with the received samples at the pilot carriers,

$$\widehat{\mathbf{H}}_{LS} = \mathbf{X}_P^{-1}\mathbf{Y}_P = \left[\frac{Y_{p-1}}{X_{p-1}} \quad \frac{Y_{2p-1}}{X_{2p-1}} \quad \cdots \quad \frac{Y_{N_P\cdot p-1}}{X_{N_P\cdot p-1}}\right]^T, \quad (2)$$

is the LS estimator of the channel frequency response at the pilot carriers, $\mathbf{R}_{HP} = E\left[\mathbf{H}\mathbf{H}_P^H\right]$ and $\mathbf{R}_{PP} = E\left[\mathbf{H}_P\mathbf{H}_P^H\right]$ are the channel correlation matrices, where $\mathbf{H}$ is a column vector with the values of the frequency response at all N carrier frequencies and $\mathbf{H}_P$ is also a column vector with the values of the frequency response at the N_P pilot frequencies.

When the noise is cyclostationary, as in PLC channels, the values of $\sigma_{U_{mp-1}}^2$ vary with time. However, it has been verified that by using their time averaged values, MSE degradation is in general very small. This result is partly a consequence of the frequency selective character of the noise time variations [1]. Since channel estimation is done by taking into account the whole set employed pilots, the effect of the noise conditions in a few of them is somehow masked by the majority of pilots in which the noise is essentially stationary.

To reduce the complexity of the estimator in (1) the term $\left(\mathbf{X}_P\mathbf{X}_P^H\right)^{-1}$ is replaced with its expectation $E\left[\left(\mathbf{X}_P\mathbf{X}_P^H\right)^{-1}\right]$ [3]. Using the same constellation in all pilots, and defining $\beta = E\left[\left|X_{mp-1}\right|^2\right]E\left[\left|1/X_{mp-1}\right|^2\right]$, with $1 \le m \le N_p$, and $\boldsymbol{\Gamma} = diag\left\{E\left[\left|X_{p-1}\right|^2\right]/\sigma_{U_{p-1}}^2, \cdots, E\left[\left|X_{N_p\cdot p-1}\right|^2\right]/\sigma_{U_{N_p\cdot p-1}}^2\right\}$, the estimator in (1) simplifies to [3]

$$\widehat{\mathbf{H}} = \mathbf{R}_{HP}\left(\mathbf{R}_{PP} + \beta\boldsymbol{\Gamma}^{-1}\right)^{-1}\widehat{\mathbf{H}}_{LS}. \quad (3)$$

The complexity of the estimator in (3), that from now on will be referred to as approximate LMMSE (aLMMSE), can be further reduced by means of two strategies [3]. The first one is to employ a low-rank approximation of the estimator matrix, obtained by means of the singular value decomposition (SVD). The second is to neglect correlation between distant pilots and to divide the symbol into blocks in which estimation is

performed independently.

To avoid exact knowledge of both the channel correlation matrices and $\mathbf{\Gamma}$, a generic design is proposed in [3]. It is based on the use of correlation matrices that are obtained for a worst-case channel with a uniform power-delay profile, and $\mathbf{\Gamma} = \mathbf{I}\gamma$, where $\mathbf{I}$ is the identity matrix and γ is fixed to a relatively high value.

To improve the performance and keep the complexity low, instead of the uniform power-delay profile assumption, we propose to employ channel statistics derived from the 24 measured channels. The frequency response of each channel has been measured in L uniformly distributed instants along the mains cycle [1]. From these measurements, the correlation matrices, $\mathbf{R}_{HP}^{i,\ell}$ and $\mathbf{R}_{PP}^{i,\ell}$, of the i-th channel during the ℓ-th instant are computed. Channel matrices employed in the aLMSSE are then obtained according to

$$\begin{aligned} \mathbf{R}_{HP} &= \frac{1}{24}\sum_{i=1}^{24}\left(\frac{1}{L}\sum_{\ell=0}^{L-1}\mathbf{R}_{HP}^{i,\ell}\right) \\ \mathbf{R}_{PP} &= \frac{1}{24}\sum_{i=1}^{24}\left(\frac{1}{L}\sum_{\ell=0}^{L-1}\mathbf{R}_{PP}^{i,\ell}\right) \end{aligned} . \tag{4}$$

Fig. 2 displays the modulus of the elements of the resulting $\mathbf{R}_{PP}$ in logarithmic scale for $p=1$. It shows typical features of indoor PLC channels. For instance, the increasing attenuation of transmission cables with frequency is clearly manifest in the decreasing character of the amplitudes in the diagonal (e.g. see the maximums). Diagonal values also reveal that notches in the frequency response are more likely in the high frequency region than, for example, in frequencies below 4MHz, where propagation distances are too short for a reflection to cause a destructive interference. The progressive shrinking of the bright regions around the diagonal as the frequency increases also reflects that correlation between tones decreases more rapidly in the high frequency region, in part because notches are more likely and appear at closer distances.

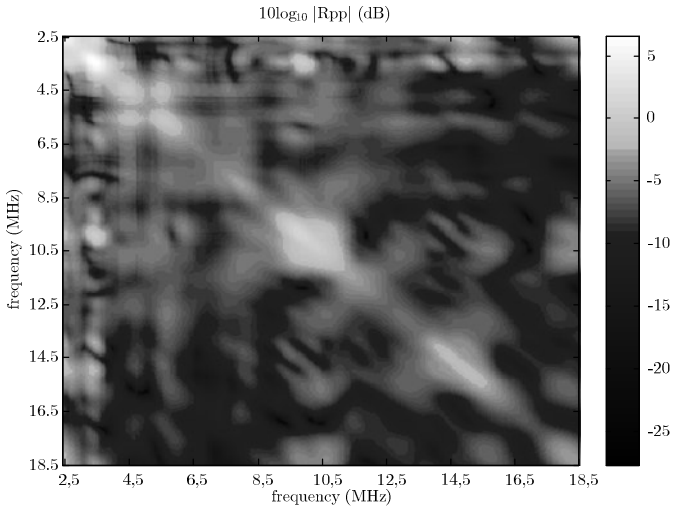

Fig. 2. Modulus of the employed $\mathbf{R}_{PP}$ in logarithmic scale for $p=1$.

D. LMS Estimator with Cubic Interpolation

The normalized LMS algorithm [7] is employed to obtain an estimate of the FEQ tap to be applied to the m-th pilot of the (n+1)-th received symbol according to

$$FEQ_{mp-1}^{n+1} = FEQ_{mp-1}^{n} + \frac{\mu \cdot e_{mp-1}^{n} \cdot \left(Y_{mp-1}^{n}\right)^{*}}{\left|Y_{mp-1}^{n}\right|^{2}}, \tag{5}$$

where $(\cdot)^{*}$ denotes the complex conjugate, Y_{mp-1}^{n} is the n-th received value in the m-th pilot and

$$e_{mp-1}^{n} = X_{mp-1}^{n} - Y_{mp-1}^{n} FEQ_{mp-1}^{n}, \tag{6}$$

where X_{mp-1}^{n} represents the n-th complex value transmitted in the m-th pilot. FEQ taps are initialized using the time-averaged values provided by the LS estimator in (2) along one mains cycle.

The algorithm in (5) uses the instantaneous power of the demodulated signal $\left|Y_{mp-1}^{n}\right|^{2}$ as an estimate of its mean value, which is an acceptable simplification for SNR values over 10dB. Based on the estimates at the pilots, FEQ taps at the remaining carriers are obtained by means of cubic interpolation. When comparing the performance of this scheme with the one given by the aLMMSE, the channel frequency response is taken as $\widehat{H}_{k}^{n} = 1/FEQ_{k}^{n}$.

The normalized step-size, μ, determines the tracking ability of the algorithm but also the magnitude of the excess error [7]. Its optimum value depends on the SNR and the Doppler spread. The higher the Doppler spread the greater μ, and the higher the SNR the lower μ.

III. Simulation Results

Performance of both channel estimation algorithms is evaluated in a system with N=512 carriers. In order to avoid ISI and ICI, the cyclic prefix length has been fixed to 300 samples at 50MHz [8], i.e. about 22.7% of the whole DMT symbol duration $(2N+cp)$. Only carriers with indexes $50 \le k \le 379$ are finally used. Pilots are modulated with 4-QAM constellations.

A. Performance of the aLMMSE Estimator

Firstly, we assess the performance obtained with the proposed average correlation matrix, and the one obtained with the uniform power-delay profile assumption. Fig. 3 depicts the MSE obtained in Ch. 1 for various pilot spacings. Although $p=1$ and $p=2$ do not have practical sense, they have been drawn to show the tendency of the performance with the pilot spacing. Curves are displayed for a wide range of SNR's, but some of them are not feasible values, since they would require an excessively high transmitted PSD. Hence, MSE values corresponding to a transmitted PSD of -

20dBm/kHz are clearly highlighted with a marker. Results obtained with the LS estimator given in (2) are drawn as a reference. Fig. 3 reveals that the proposed channel statistics outperforms the uniform power-delay profile design, which experiences severe MSE penalty at high SNR, where channel model mismatch becomes the limiting factor. Degradation caused by the pilot spacing depends on the SNR. At lower SNR, estimation errors are mainly driven by the channel noise, but at high SNR, the pilot spacing becomes the limiting term.

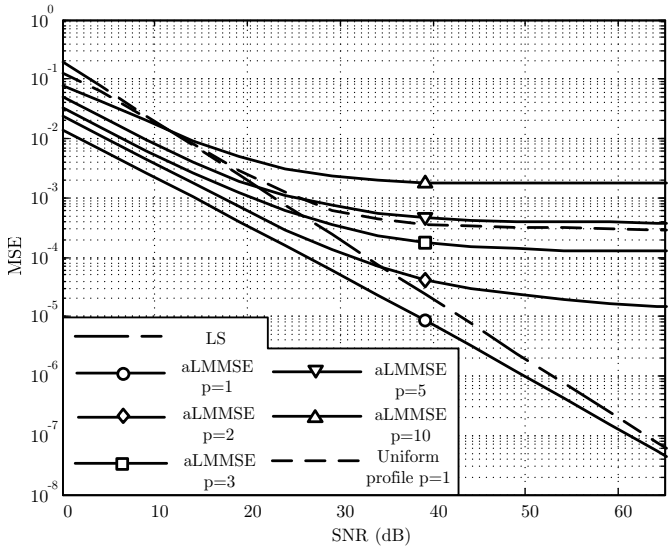

Fig. 3. MSE of the aLMMSE in Ch. 1 for various pilot spacings.

To illustrate the effect of employing a low rank approximation of the estimator in (3) based on the SVD and the use of a predefined $\mathbf{\Gamma}$ with a fixed value of γ, Fig. 4 depicts the MSE in Ch. 1 for pilot spacings $p=2$ and $p=10$ in the following cases: the aLMMSE estimator with no rank reduction and with actual $\mathbf{\Gamma}$, the aLMMSE with rank-q (q=40 and q=100) with actual $\mathbf{\Gamma}$ and the aLMMSE with rank-q (q=40 and q=100) and $\gamma=50\text{dB}$. It can be observed that a rank-100 estimator with actual values of $\mathbf{\Gamma}$ offers the same performance as the aLMMSE without rank reduction in all cases (curves are indistinguishable). On the other hand, a rank-40 estimator limits the performance when the pilot spacing is small. Regarding the effect of using a fixed γ, in the high SNR regime it causes an error floor that appears when the elements of $\mathbf{\Gamma}$ become greater than γ (see the rank-100 estimator with $\gamma=50\text{dB}$ and $p=2$). In the low SNR regime it increases the MSE.

Degradation caused by dividing the symbol into *M* blocks in which estimations is performed independently is shown in Fig. 5. The MSE obtained in Ch. 1 and Ch.2 for pilot spacings $p=2$ and $p=10$ is represented for $M=1$, $M=3$ and $M=11$. The average channel statistic with $\gamma=50\text{dB}$ is employed in all cases. Firstly, it is interesting to observe that, for high SNR and $M=1$, MSE values obtained in Ch. 2 are smaller than the ones in Ch. 1. This is consistent with the fact that Ch. 2 exhibits a higher coherence bandwidth than Ch. 1. This reason is also responsible for the reduced performance degradation that occurs in Ch. 1 for $p=2$ when the symbol is divided into blocks. Since pilots that are further apart are nearly uncorrelated, performance is almost unaltered when they are not taken into account. It is worth noting that neglecting information provided by pilots in adjacent blocks degrades the performance when the SNR is high. However, when the SNR is low, noise introduced by distant pilots is higher than the information they provide and the MSE improves when dividing the symbol into blocks.

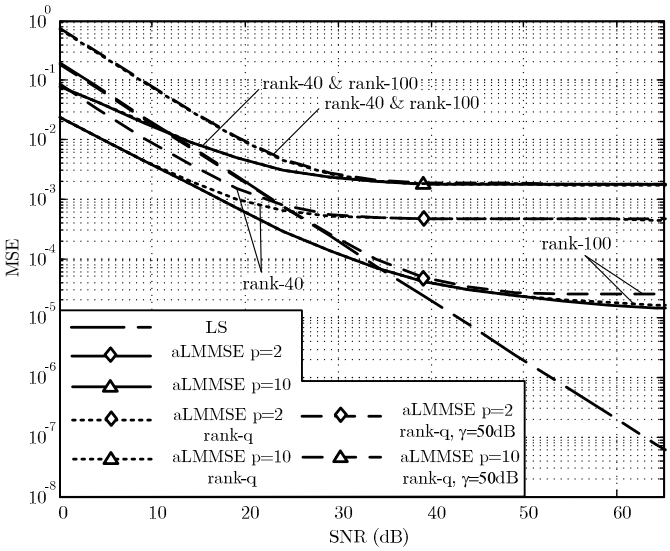

Fig. 4. MSE of the aLMMSE in Ch. 1 for various ranks and predefined γ.

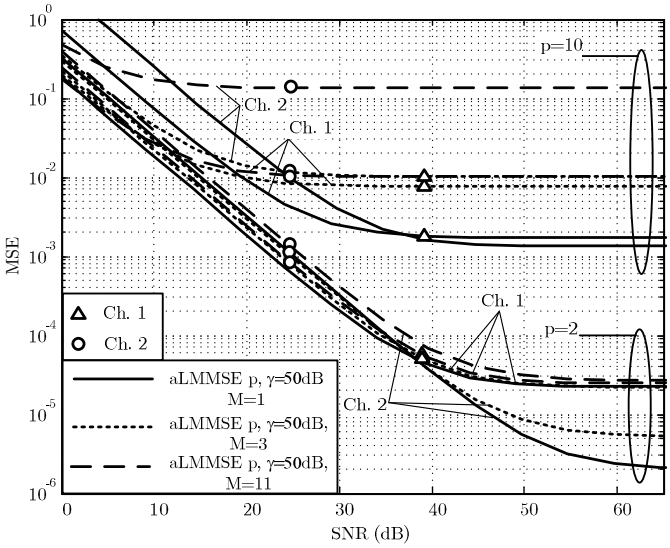

Fig. 5. MSE of the aLMMSE in Ch. 1 and Ch. 2 for various block sizes and pilot spacings.

B. Performance of the LMS Estimator

Fig. 6 depicts MSE values obtained in Ch.1 and Ch. 2 with $p=1$, $p=2$ and $p=10$ when using $\mu=0.1$ and $\mu=0.9$.

Firstly, let's concentrate in Ch. 1. It can be observed that for low SNR values, $\mu = 0.1$ provides better results than $\mu = 0.9$ because channel noise dominates over tracking errors. When SNR increases, the tracking capacity of the LMS becomes the limiting factor and $\mu = 0.9$ is the most appropriate step-size. Surprisingly, MSE values obtained in Ch. 1 at high SNR's are always lower than the ones in Ch. 2. This is in contradiction with results obtained with the aLMMSE for $p = 2$ and also with the smaller coherence bandwidth of Ch. 1. The reason is the mediocre performance of the LMS when tracking the type of time variations exhibited by Ch. 2. This can be clearly observed in Fig. 7 (a), where the values of Ch. 1 and Ch.2 frequency response along the mains cycle have been represented in the complex plane for two frequencies. Fig. 7 (b) depicts the modulus of the frequency responses shown in Fig. 7 (a) and the corresponding estimates obtained with the LMS. As seen, Ch. 1 variations occur mainly in the modulus, while in Ch. 2 they are essentially due to phase variation. Note that Ch.2 amplitude variations are smaller than 2dB (Ch. 2 has lower mean Doppler spread values because of the remarkable frequency selectivity of its time variations). Fig. 7 (b) shows that the LMS is able to track considerable modulus variations (actual and estimated channel are indistinguishable), but performs very poorly when tracking phase changes. The remarkable phase changes in Ch. 2 frequency response are also responsible for the severe degradation performance observed in Fig. 5 for the aLMMSE with $M = 11$.

Comparing MSE values in Fig. 6 with the ones in Fig. 5 for $M = 3$, it can be observed that the LMS with a proper step-size selection provides similar performance to the aLMMSE. A remarkable exception is Ch. 2 with $p = 10$, where the aLMMSE gives MSE values one order of magnitude lower than the ones of the LMS. However, in terms of bit-rate, the LMS outperforms the aLMMSE even in these circumstances, as it will be shown in the next subsection.

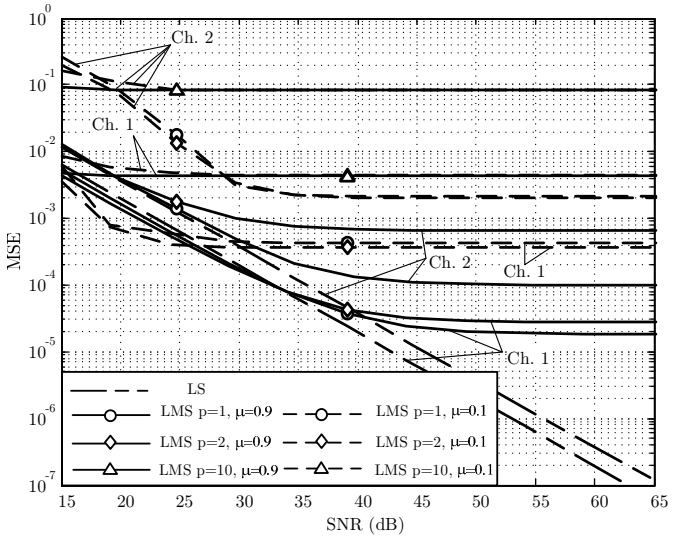

Fig. 6. MSE of the LMS in Ch. 1 and Ch. 2 as for various step-sizes and pilot spacings.

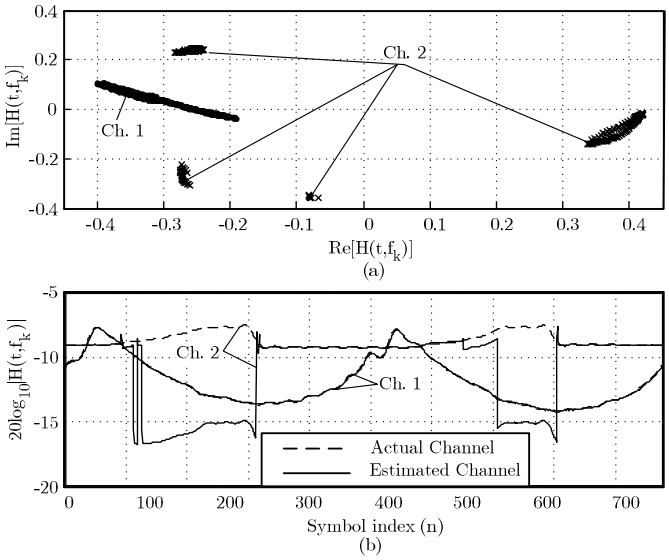

Fig. 7. (a) Real and imaginary part of the frequency response of Ch. 1 at 3.8MHz and of Ch. 2 at 9.7MHz, (b) modulus of the actual and estimated values of the frequency responses in (a).

C. Performance Comparison

Estimators are now compared in terms of symbol error probability (SER) and attained bit-rate. Carriers not used as pilots are loaded with BPSK and square QAM constellations subject to an objective symbol error rate (SER) of 10^{-4} and a maximum of 16 bits per symbol. Constellations are selected according to the signal to noise and distortion ratio (SNDR), calculated by averaging over one mains cycle. The SNDR includes the noise and the distortion caused by channel estimation errors. Both of them are assumed to be independent and Gaussian. A 3dB system margin is included in all cases.

Fig. 8 depicts the bit-rate values attained in Ch.1 and Ch.2 when using the LMS and aLMMSE with $M = 3$, $\gamma = 50$dB. In the LMS case, since the most appropriate step-size (in terms of the MSE) is different for each channel, an intermediate value of $\mu = 0.5$ has been utilized. Realistic transmitted PSD's values in the range from -40dBm/kHz to -20dBm/kHz have been employed. In these circumstances, the measured noise instantaneous PSD's and channel responses of the selected channels are such that the averaged SNR in Ch. 1 ranges from 18.91dB to 38.91dB and from 4.39dB to 24.39dB in Ch. 2.

It can be easily shown that the complexity of the selected aLMMSE is higher than the one of the LMS [3]. In spite of this, the LMS outperforms the aLMMSE algorithm in all cases, as observed in Fig. 8. The situation is particularly interesting in Ch. 2, where the aLMMSE exhibits lower MSE values than the LMS. As previously mentioned, the reason for the inferior performance of the LMS is its poor performance in a small number of carriers in which the frequency response experienced remarkable phase. However, these carriers remain empty after the bit-loading procedure and, in the remaining ones, the LMS has better performance. As a reference, an ideal

pilot-based system (perfect channel estimation) with $p=10$ and a transmitted PSD of -20dBm/kHz would achieve 87.7Mbit/s in Ch. 1 and 41.4Mbit/s in Ch. 2.

The optimum pilot spacing results from the trade-off between estimation errors and transmission efficiency. Although Fig. 8 only displays two pilot spacings, it reveals that $p=10$ is an appropriate value.

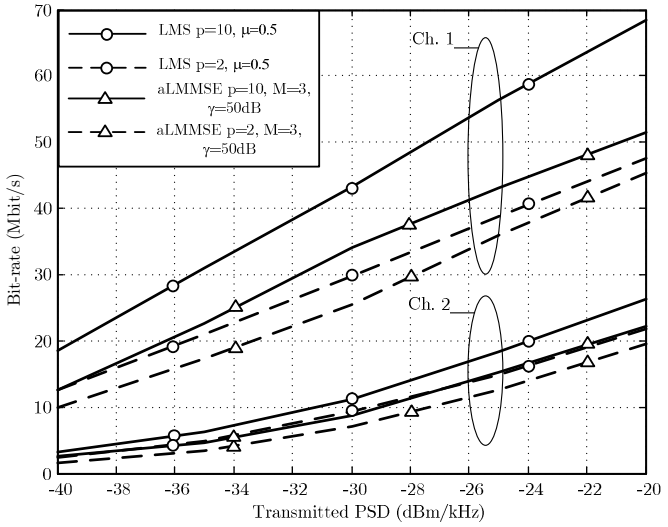

Fig. 8. Bit-rates attained in Ch. 1 and Ch. 2 with the aLMMSE and the LMS.

Exact values of the SER measured during data transmission phase are shown in Fig. 9 (a) for Ch. 1 and Fig. 9 (b) for Ch. 2. Results displayed in Fig. 9 (a) explain the increasing bit-rate differences between the LMS and the aLMMSE in Ch. 1 for large transmitted PSD's and $p=10$. As seen, SER values achieved by the aLMMSE are much lower than the ones of the LMS. Therefore, the bit-rates of the aLMMSE can still be improved without exceeding the objective SER. However, it is worth noting that a practical system would not be able to obtain this improvement without violating the SER constraint in Ch. 2. Fig. 9 (a) and (b) also show that the SER obtained with the LMS is higher than the objective one in some situations. However, since the difference is small, this problem can be solved with minimum bit-rate degradation by using a slightly larger system margin.

IV. Conclusion

In this work, pilot-based channel estimation techniques based on an approximate LMMSE (aLMMSE) and on the LMS with cubic interpolation between tones have been compared.

We have shown that a generic aLMMSE estimator based on average channel statistics derived from measurements outperforms the one based on a uniform power-delay profile. Further, the performance degradation caused by using a rank-100 estimator in a system with 512 carriers is negligible. Similarly, performance remains nearly unaltered when dividing the symbol into 3 blocks in which estimation is performed independently.

The LMS can track channels with remarkable amplitude variations but performs poorly when tracking phase changes. Nevertheless, when a bit-loading procedure is employed, the LMS attains higher bit-rates than the aLMMSE with reduced computational complexity.

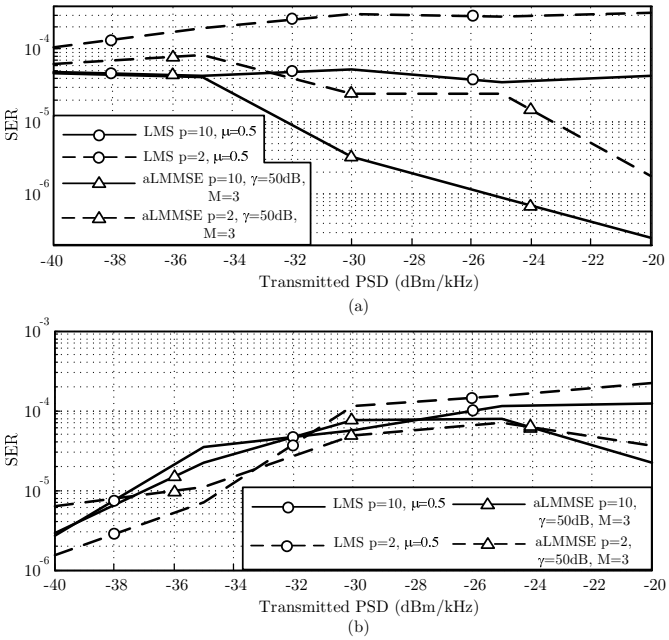

Fig. 9. SER in (a) Ch.1 and (b) Ch.2.

References

[1] F. J. Cañete, J. A. Cortés, L. Díez and J. T. Entrambasaguas, "Analysis of the Cyclic Short-Term Variation of Indoor Power-line Channels," IEEE Journal on Selected Areas on Communications, Vol. 24, No. 7, July 2006, pp. 1327-1338.

[2] Y. Li, L. J. Cimini and N. R. Sollenberger, "Robust Channel Estimation for OFDM Systems with Rapid Dispersive Fading Channels," IEEE Transactions on Communications, Vol. 46, No. 7, July 1998, pp. 902-915.

[3] O. Edfors, M. Sandell, J.J. van de Beek, S. K. Wilson and P. O. Börjesson, "OFDM Channel Estimation by Singular Value Decomposition," IEEE Transactions on Communicatons, Vol. 46, No. 7, July 1998, pp. 931-939.

[4] M. Hsieh and C. Wei, "Channel Estimation for OFDM Systems Based on Comb-Type Pilot Arrangement in Frequency Selective Fading Channels," IEEE Transactions on Consumer Electronics, Vol. 44, No. 1, Feb. 1998, pp. 217-225.

[5] S. Coleri, M. Ergen, A. Puri and A. Bahai, "Channel estimation techniques based on pilot arrangement in OFDM systems," IEEE Transactions on Broadcasting, Vol. 48, Issue 3, Sept. 2002 , pp. :223-229.

[6] J. M. Cioffi, "A Multicarrier Primer, "Amati Communications Corporation and Stanford University, ANSI T1E1.4/91-157 Committee Contribution, November, 1991.

[7] S. Haykin, "Adaptive Filter Theory," Second Edition, Prentice-Hall.

[8] F. J. Cañete, J. A. Cortés, L. Díez and J. T. Entrambasaguas, "Modeling and Evaluation of the Indoor Power Line Channel," IEEE Communications Magazine, Vol. 41, Issue 4, April 2003, pp. 41.47.